Opto-Electronic Science

CN 51-1800/O4 ISSN 2097-0382 (Print) ISSN 2097-4000 (Online)

Aberration-corrected differential phase contrast microscopy with annular illuminations

Yao Fan, Chenyue Zheng, Yefeng Shu, Qingyang Fu, Lixiang Xiong, Guifeng Lu, Jiasong Sun, Chao Zuo and Qian Chen

Citation: Fan Y, Zheng CY, Shu YF, et al. Aberration-corrected differential phase contrast microscopy with annular illuminations. *Opto-Electron Sci* **x**, 240037 (2025).

https://doi.org/10.29026/oes.2025.240037

Received: 27 December 2024; Accepted: 19 February 2025; Published online: 6 June 2025

Related articles

Cascaded metasurfaces enabling adaptive aberration corrections for focus scanning

Xiaotong Li, Xiaodong Cai, Chang Liu, Yeseul Kim, Trevon Badloe, Huanhuan Liu, Junsuk Rho, Shiyi Xiao

Opto-Electronic Advances 2024 **7**, 240085 doi: 10.29026/oea.2024.240085

Cascaded metasurfaces for adaptive aberration correction

Lei Zhang, Tie Jun Cui

Opto-Electronic Advances 2025 **8**, 250052 doi: 10.29026/oea.2025.250052

Deep learning assisted variational Hilbert quantitative phase imaging

Zhuoshi Li, Jiasong Sun, Yao Fan, Yanbo Jin, Qian Shen, Maciej Trusiak, Maria Cywińska, Peng Gao, Qian Chen, Chao Zuo

Opto-Electronic Science 2023 **2**, 220023 doi: 10.29026/oes.2023.220023

Design, setup, and facilitation of the speckle structured illumination endoscopic system

Elizabeth Abraham, Zhaowei Liu

Opto-Electronic Science 2025 **4**, 240022 doi: 10.29026/oes.2025.240022

Opto-Electronic Science

Article

xxxx 2025, Vol. x, No.

DOI: 10.29026/oes.2025.240037 CSTR: 32246.14.oes.2025.240037

Aberration-corrected differential phase contrast microscopy with annular illuminations

Yao Fan[1,2,3†], Chenyue Zheng[1,2,3†], Yefeng Shu[1,2,3], Qingyang Fu[1,2,3], Lixiang Xiong[1,2,3], Guifeng Lu[1,2,3], Jiasong Sun[1,2,3*], Chao Zuo[1,2,3*] and Qian Chen[1,2,3*]

Quantitative phase imaging (QPI) enables non-invasive cellular analysis by utilizing cell thickness and refractive index as intrinsic probes, revolutionizing label-free microscopy in cellular research. Differential phase contrast (DPC), a non-interferometric QPI technique, requires only four intensity images under asymmetric illumination to recover the phase of a sample, offering the advantages of being label-free, non-coherent and highly robust. Its phase reconstruction result relies on precise modeling of the phase transfer function (PTF). However, in real optical systems, the PTF will deviate from its theoretical ideal due to the unknown wavefront aberrations, which will lead to significant artifacts and distortions in the reconstructed phase. We propose an aberration-corrected DPC (ACDPC) method that utilizes three intensity images under annular illumination to jointly retrieve the aberration and the phase, achieving high-quality QPI with minimal raw data. By employing three annular illuminations precisely matched to the numerical aperture of the objective lens, the object information is transmitted into the acquired intensity with a high signal-to-noise ratio. Phase retrieval is achieved by an iterative deconvolution algorithm that uses simulated annealing to estimate the aberration and further employs regularized deconvolution to reconstruct the phase, ultimately obtaining a refined complex pupil function and an aberration-corrected quantitative phase. We demonstrate that ACDPC is robust to multi-order aberrations without any priori knowledge, and can effectively retrieve and correct system aberrations to obtain high-quality quantitative phase. Experimental results show that ACDPC can clearly reproduce subcellular structures such as vesicles and lipid droplets with higher resolution than conventional DPC, which opens up new possibilities for more accurate subcellular structure analysis in cell biology.

Keywords: quantitative phase imaging; differential phase contrast; aberration-corrected; annular illumination

Fan Y, Zheng CY, Shu YF et al. Aberration-corrected differential phase contrast microscopy with annular illuminations. *Opto-Electron Sci* **x**, 240037 (2025).

Introduction

Light microscopy plays a crucial role in biomedical research, pharmaceutical discovery, and materials science by providing visual images and data of biological cells to support analyses of key properties such as morphological features, internal structure, dynamic behavior, and functional change[1–4]. Recent advances in biological cell research have greatly facilitated the widespread application of label-free microscopy at the cellular and subcellular scales[5–8]. Phase encodes essential information about

[1]Smart Computational Imaging Laboratory (SCILab), School of Electronic and Optical Engineering, Nanjing University of Science and Technology, Nanjing 210094, China; [2]Smart Computational Imaging Research Institute (SCIRI) of Nanjing University of Science and Technology, Nanjing 210019, China; [3]Jiangsu Key Laboratory of Visual Sensing & Intelligent Perception, Nanjing 210094, China.

[†]These authors contributed equally to this work.

*Correspondence: JS Sun, E-mail: sunjiasong@njust.edu.cn; C Zuo, E-mail: zuochao@njust.edu.cn; Q Chen, E-mail: chenqian@njust.edu.cn

Received: 27 December 2024; Accepted: 19 February 2025; Published online: 6 June 2025

the optical path length differences induced by samples[9], providing a non-invasive means to quantify refractive index and thickness distributions. Capitalizing on this physical property, quantitative phase imaging (QPI) utilizes phase (Thickness) as an endogenous "probe" to reconstruct cellular morphology and biophysical parameters without phototoxic effects, opening up new ways to explore the cellular microcosm[10–15]. As one of the most promising QPI techniques, differential phase contrast (DPC) exploits the phase transfer properties of asymmetric illumination and recovers the sample's phase by solving the inverse problem[16–18]. It requires only four intensity measurements to obtain the quantitative phase with high robustness and high lateral resolution reaching to the incoherent diffraction limit, demonstrating powerful imaging capabilities in cell applications[19, 20].

Although DPC is an important advancement in non-interferometric QPI, its reconstruction algorithm poses challenges because it requires accurate physical modeling from intensity to phase[19,21]. DPC employs the phase transfer function (PTF) to quantitatively characterize the relationship between the intensity signal and the object phase, which is modeled as a multidimensional integral of the illumination with the pupil function of the system[22]. The undesired aberration as the phase term of the pupil function alters the PTF response and may deteriorate image results[23]. Commercial microscopes are designed to minimize the effects of aberration as much as possible by optimizing the optical system, but unavoidable system defects and disturbances from external environments may cause pupil to deviate from the ideal value, resulting in severe phase distortion, blurring, and artifacts. To address this problem, the sample-independence nature of aberration motivates wavefront sensing and adaptive optics to be introduced into QPI to pre-estimate and quantify the system aberration prior to data acquisition[24, 25]. However, the specific wavefront sensor devices and the additional aberration estimation step increase the complexity and technical challenges of the phase reconstruction process.

Advances in phase retrieval algorithms have opened up new ways to jointly recover sample phase and system aberration from raw intensities without any additional hardware, with the advantages of automatic correction and wide sample adaptability[26–31]. Inspired by this idea, self-correcting methods have been developed in QPI techniques to ensure high-quality, artifact-free output phases. Fourier ptychographic microscopy (FPM) employs alternating projection (AP) iterations to simultaneously recover the phase of the object and the aberration, thus obtaining high-resolution complex field information with a large field of view[32–35]. The AP is also utilized in DPC to recover the complex transmittance function of the object as well as the aberration using only four intensity images (Three asymmetric illuminations and a collimated incident illumination)[36]. Nevertheless, its aberration retrieval relies heavily on the sensitivity of the additionally acquired images under the collimated illumination (Coherent illumination) to the aberration. Moreover, the use of half-circular illumination results in a small PTF response at low frequencies and high frequencies approaching $2NA_{\mathrm{obj}}$, which in turn limits the imaging resolution and signal-to-noise ratio (SNR). Recently, the annular illumination with illumination numerical aperture (NA) matching the NA of the objective lens has been identified provides an optimal (spectrum coverage and transfer response) phase transfer response for high-resolution, high-contrast reconstructed phase with less data requirements[37–39].

We propose an artifact-free aberration-corrected DPC (ACDPC) QPI method grounded in the annular illumination (Optimized PTF) and leveraging simulated annealing to solve the optimization problem for aberration retrieval. Consequently, only three acquired data frames are required to reconstruct both the object phase and the complex pupil function, achieving aberration-free, high-resolution QPI. Phase retrieval is facilitated by an iterative deconvolution algorithm, which incorporates simulated annealing for aberration estimation and a tempering process to expedite convergence, ultimately resulting in a refined complex pupil function and an aberration-corrected quantitative phase. Furthermore, we analyze the data redundancy requirements and propose a minimum data scheme for ACDPC, i.e., at least three images are required to recover phase and aberration simultaneously. Both simulations and experiments validate that the proposed ACDPC method is robust against 5th-order aberrations and ensures high-quality quantitative phase reconstruction. ACDPC achieves artifact-free, high-resolution QPI, demonstrating its adaptability to various optical microscope systems, paving the way for practical applications in biological research.

Method

Phase transfer modeling with complex pupil function

DPC, a technique with partially coherent imaging,

employs asymmetric half-circular illuminations to sequentially illuminate the sample, capturing two phase contrast images for each shearing direction. The acquired intensity image is bilinearly related to the object information. In order to establish an explicit expression of the intensity and object distributions, the weak object approximation $t(\boldsymbol{x}) = \exp[\mathrm{i}\phi(\boldsymbol{x})] \approx 1 + \mathrm{i}\phi(\boldsymbol{x})$ (which requires that the phase perturbation of the sample to the incident light be sufficiently weak) is introduced to linearize the phase distributions of the intensity signals with the object. Then, the acquired intensity can be expressed as a superposition of the DC component with the product of the phase $\Phi(\boldsymbol{u})$ of the object and the corresponding transfer function (the derivation of the intensity expression for partially coherent imaging under the weak scattering approximation can be found in Section 1 of Supplementary information)[21]:

$$I(\boldsymbol{x}) = F^{-1}\left[B\delta(\boldsymbol{u}) + \mathrm{i}\mathrm{PTF}(\boldsymbol{u})\,\Phi(\boldsymbol{u})\right], \tag{1}$$

where $I(\boldsymbol{x})$ is the acquired intensity, and $B\delta(\boldsymbol{u})$ is the DC component. $\mathrm{PTF}(\boldsymbol{u})$ is the PTF that characterizes the quantitative relationship between the phase of an object and the captured intensity signal:

$$\mathrm{PTF}_{lr}(\boldsymbol{u}) = \frac{\iint S_{lr}(\boldsymbol{u}_j)\left[P^*(\boldsymbol{u}_j)P(\boldsymbol{u}+\boldsymbol{u}_j) - P(\boldsymbol{u}_j)P^*(\boldsymbol{u}_j-\boldsymbol{u})\right]\mathrm{d}^2\boldsymbol{u}_j}{\iint |S_{lr}(\boldsymbol{u}_j)|\,|P(\boldsymbol{u}_j)|^2\,\mathrm{d}^2\boldsymbol{u}_j}, \tag{2}$$

here $S(\boldsymbol{u})$ represents the illumination function, $P(\boldsymbol{u})$ denotes the complex pupil function of the system. Ideally, the pupil function is modeled as a uniformly distributed low-pass filter (with a cutoff frequency of 1 inside and 0 outside, and its cutoff frequency is determined by the NA of the objective lens NA_{obj} and the illumination wavelength λ) to independently analyze the effect of illumination on the PTF. Our prior research analyzed the relationship between the illumination and the PTF of DPC, revealing that annular illumination (Illumination NA equal to the objective NA) substantially boosts the PTF response across the entire incoherent diffraction bandwidth[37,38,40]. According to Eq. (2), the PTF under a single illumination is a superposition of two shifted pupil functions with opposite values[37]. When the illumination angle corresponds to a lower spatial frequency, the PTF responses of the overlapping parts cancel each other out. As a result, conventional half-circular illumination implies a narrower frequency range and weaker PTF values. The annular illumination ($NA_{\mathrm{ill}} = NA_{\mathrm{obj}}$) produces the optimal PTF, which is tangent to the two apertures, offering maximum spectrum coverage and uncut values (As in the left half of Fig. 1(b) and 1(c)).

When there is aberration in the system, $P(\boldsymbol{u})$ is a complex pupil function whose amplitude is the circular aperture while the aberration is contained in the phase. This complex pupil function leads to a change in the PTF response with characteristics different from those of the ideal pupil. As depicted in Fig. 1, the PTFs for different illumination angles in the complex pupil function are no longer completely numerically symmetric. Consequently, the overlapping parts of the PTF do not cancel each other out, which provides a theoretical basis for enhancing the PTF response at low frequencies by modulation of the pupil. However, this asymmetric response of PTF also increases the complexity of the pupil retrieval, which is the reason why QPI techniques for partially coherent imaging have difficulty in resolving aberrations directly. Furthermore, we present the PTF associated with the complex pupil function under half-circular and half-annular illuminations, as shown in the right half of Fig. 1(c). Compared to the ideal pupil condition, the presence of aberrations reduces PTF response in both illumination modes. Crucially, however, half-annular illumination demonstrates measurable response improvements over half-circular illumination under aberration conditions, highlighting its universal applicability in achieving high-quality phase reconstruction through optimized PTF spectrum coverage and enhanced transfer response characteristics. This half-annular illumination will be used as an illumination optimization strategy for correcting aberrations, providing new insights for quantitative studies of samples in the presence of aberrations.

Artifact-free aberration-corrected DPC method

In an actual microscope system, defects in the optical system and external environment disturbances introduce undesired optical aberrations[41,42], which are manifested as phase terms in the pupil function. Thus, the pupil function can be modeled as a weighted sum of Zernike polynomials[43–45], parameterized by a small number of coefficients:

$$P(\boldsymbol{u}) = \mathrm{circ}(\boldsymbol{u})\exp\left[\mathrm{i}\sum_{m=0}^{M} c_m Z_m\right], \tag{3}$$

where $c_m Z_m$ denotes the Zernike polynomial, and Z_m is the M-th Zernike modes. Substituting the complex pupil

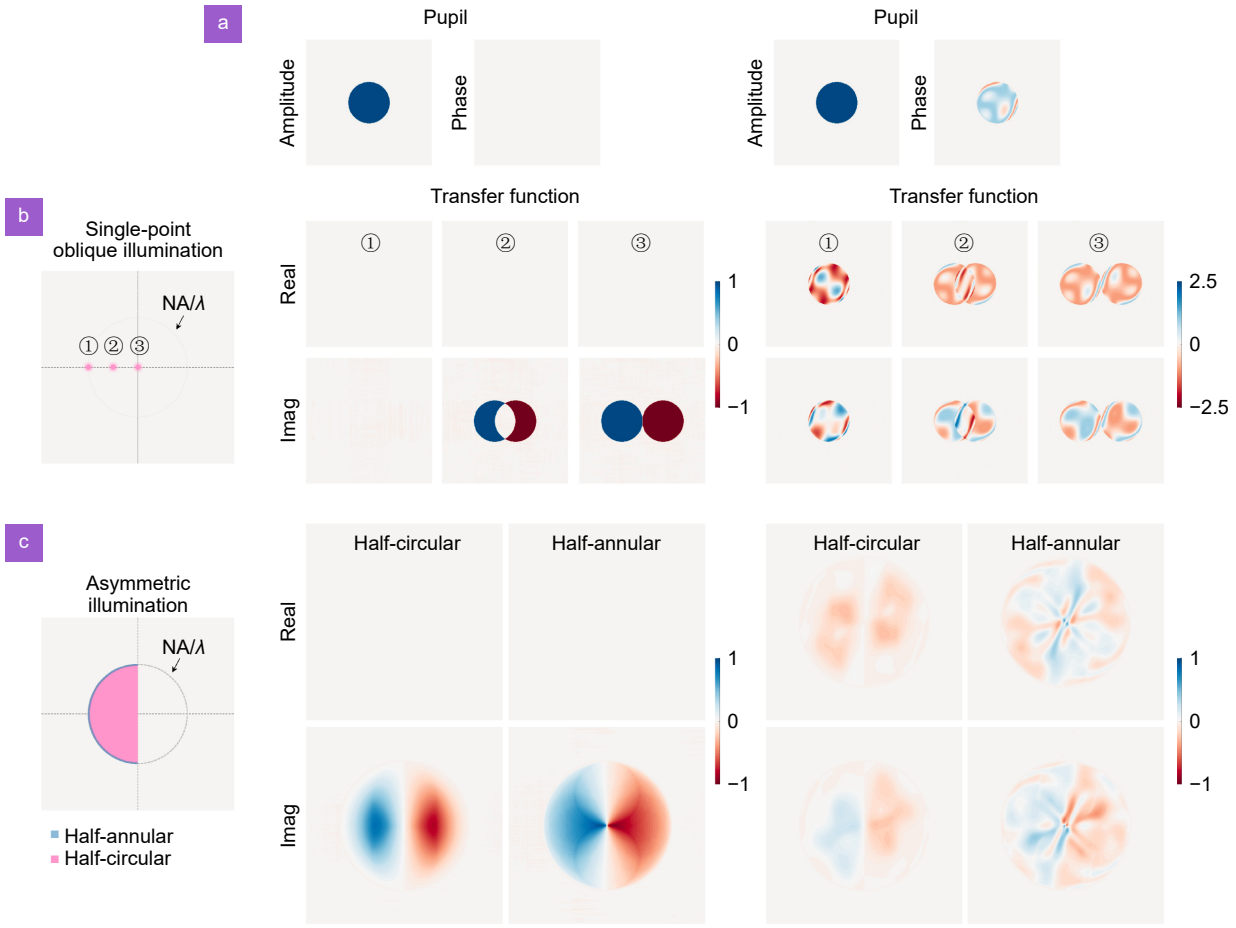

Fig. 1 | PTF with ideal pupil and complex pupil under different illuminations. (**a**) Ideal pupil without aberration and complex pupil with aberration for simulation. (**b**) Comparison of PTFs with ideal pupil and complex pupil under single point illumination at different angles. (**c**) Comparison of PTFs with ideal pupil and complex pupil under half-circular and half-annular (NA_{ill} = NA_{obj}) illuminations.

function into the PTF expression in Eq. (2), the resulting response in the overlapping regions no longer stacks to cancel each other out and retains certain transfer properties. As a result, the complex pupil changes the symmetry of the PTF, complicating the derivation of the pupil and illumination from the PTF[46]. However, a benefit is that the complex pupil function prevents the PTF from canceling out under mismatched illumination, which would open up the possibility of accurate QPI under relaxed illumination.

Consider the PTF under complex pupil is expressed as a 2D integral of the illumination and pupil functions, which is coupled with the object information in the intensity signal[16]. Consequently, solving for both the object phase and pupil functions analytically is a great challenge. ACDPC uses three annular illuminations to acquire data for system aberration retrieval and sample phase recovery. Specifically, three annular illumination patterns with $S(\boldsymbol{u}) = \delta(\boldsymbol{u} - \boldsymbol{u}_j)$ $(|\boldsymbol{u}_j| = NA_{obj}/\lambda)$ 120° apart are sequentially lit to obtain three intensity images, as shown in Fig. 2(b). They are aligned with three distinct shearing directions to achieve full spectrum coverage of the intensity measurements. We further propose an iterative reconstruction algorithm that incorporates embedded annealing and tempering processes for aberration correction to simultaneously address the tasks of phase recovery and aberration retrieval. Specifically, the pupil function is iteratively refined by annealing and tempering algorithms to estimate the system aberration, resulting in a PTF considering the actual aberrations, which is subsequently employed for deconvolution reconstruction to solve the inverse problem of DPC. The phase reconstruction with aberration correction is considered as solving the optimization problem with a cost function is defined as:

$$\min_{\phi,c} f(\boldsymbol{u}) = \sum_{j=1}^{3} \frac{\left\| I_j(\boldsymbol{u}) - \mathrm{PTF}_j(\boldsymbol{u};c)\,\phi(\boldsymbol{u}) \right\|_2^2}{\left\| I_j(\boldsymbol{u}) \right\|_2^2}, \qquad (4)$$

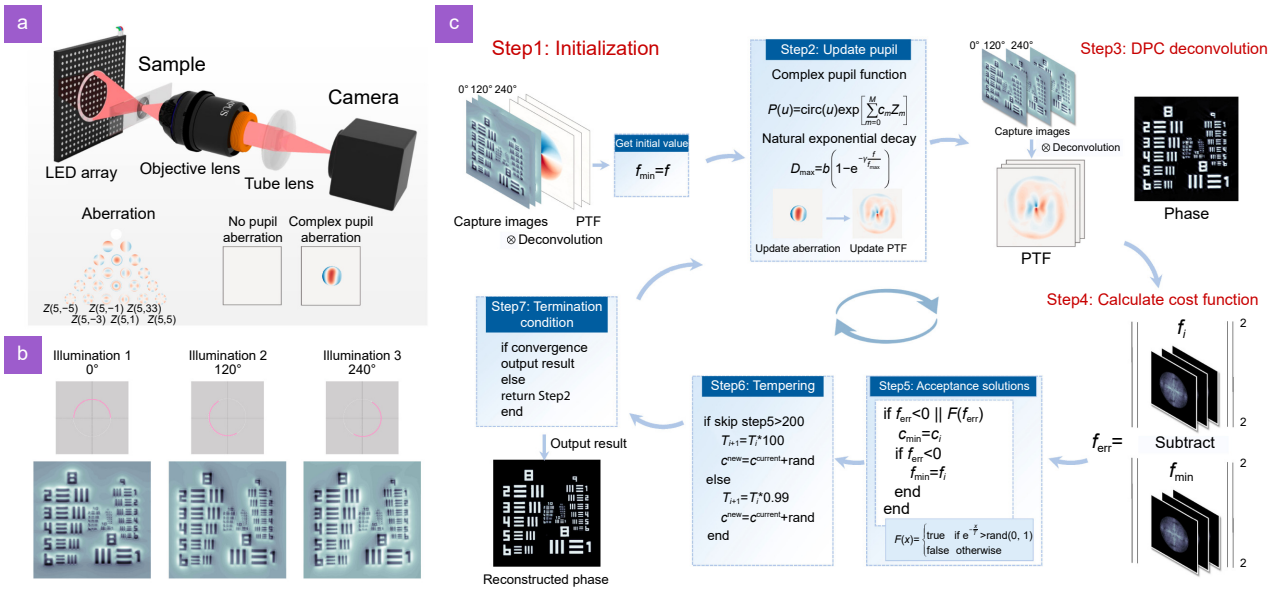

Fig. 2 | The flowchart of ACDPC iterative reconstruction joint optimization algorithm. (**a**) ACDPC imaging system based on half-annular illumination. (**b**) Three annular illumination patterns and their intensity images. (**c**) The flowchart of ACDPC method.

where j denotes the index of intensity image after removing the DC term from the original image. The deconvolution reconstruction of DPC is performed by the Tikhonov regularization[47]:

$$\phi^{k+1}(\boldsymbol{x}) = F^{-1}\left\{\frac{\sum_{j=1}^{3}\left[\mathrm{PTF}_j^*(\boldsymbol{u},c_k)\cdot I_j(\boldsymbol{u})\right]}{\sum_{j=1}^{3}\left|\mathrm{PTF}_j^*(\boldsymbol{u},c_k)\right|^2+\beta}\right\}, \quad (5)$$

β represents the regularization parameter to avoid excessive amplification of noise. Due to the asymmetry of the PTF under complex pupil, the intensity spectrum residual under different illuminations will decrease as updated aberration converges to the true value. Thus, the cost function will guide the pupil function to approximate towards the real aberration, thus simultaneously estimating the accurate PTF and reconstructed phase. Furthermore, we delve into the minimum data requirements for retrieving both the pupil function and the object phase, determining that acquiring data under three annular illuminations would yield the least raw data while still effectively decoupling phase and aberration information (The simulation analysis of data redundancy can be found in Section 3 in the Supplementary information).

The flowchart of ACDPC joint optimization algorithm, which incorporates an embedded annealing-tempering aberration correction, is illustrated in Fig. 2. The algorithm starts with a conventional DPC reconstruction, which performs a deconvolution reconstruction by setting the initial Zernike coefficients to zero to obtain the initial phase for subsequent iterations. This initial phase is used to calculate f as the initial $f_{\min}$ according to Eq. (4). During each iteration, the Zernike coefficients are refined by generating random values within an adaptively adjusted range, which is used to update the PTF and thus perform phase reconstruction. The estimated phase and the updated pupil are then utilized to generate the estimated intensity through the transfer function method, which is used for the evaluate of the cost function in Eq. (4). The newly updated pupil function is accepted depending on the change in the cost function using the Metropolis criterion as the importance sampling judgment method. We design a learning rate decay strategy based on natural exponential decay to optimize the search process (The details can be seen in Section 2 of the Supplementary information). During initial iterations, gradual contraction of the search range ensures thorough global exploration to prevent premature convergence to local optima. As the cost function values progressively diminish, the search range undergoes rapid contraction, facilitating concentrated local exploitation near potential optimal solutions. This dynamic adjustment mechanism sustains robust global search capabilities in early phases while transitioning to intensified local exploitation during later iterations, thereby enhancing solution precision and convergence rate through systematic space refinement. The iterative process will be performed several times until the reconstructed phase and estimated aberration generate an estimated intensity

with negligible difference from the acquired image. Furthermore, to prevent ACDPC from getting stuck in local minima, a tempering process is incorporated to allow the algorithm to escape from the local optimum trap when the loop termination condition is not met and no new solution has been accepted for a specified number of iterations. In comparison to existing aberration recovery algorithms, ACDPC retrieves the aberration of the system without requiring any physical prior information and achieves high-quality quantitative phase imaging with aberration correction.

Simulation results for different aberrations

Optical system aberrations usually originate from the imperfect design of the optical system and improper setting of system parameters. In existing commercially available microscopes, defocus aberrations are the most commonly encountered challenge as aberrations such as spherical or chromatic aberration are usually mitigated to the greatest extent possible at the optical design stage. Significant defocus aberrations were introduced in the objective pupil using an Abbe-based model to generate intensity images along three shearing directions under annular illumination. The complex transmittance function of the object is constructed here to consider purely phase objects where the amplitude remains constant, with the phase serving as the resolution target for the USAF. Suppose that such a sample is illuminated at a wavelength of 525 nm, and the light field through the sample is collected by a 20×, 0.4 *NA* objective lens, and finally imaged on a sensor with a pixel size of 1.85 μm.

We firstly compared the reconstructed phase of the conventional DPC method (Four half-circular illuminations) and ACDPC method (Three annular illuminations) with defocus aberration (Fig. 3). In DPC, the defocus aberration causes the phase details to be distorted, while ACDPC is highly robust to varying levels of aberration, yielding high-quality reconstructed phase reaching the theoretical resolution of the incoherent diffraction limit. The result with a defocus aberration coefficient of 2 was selected to zoom in for further demonstration and comparison, and the results are displayed in Fig. 3(b). The uniform pupil of the conventional DPC fails to account for the actual defocus aberration, leading to a mismatch between its PTF and intensity signal, which eventually results in severe distortion of the reconstructed phase. ACDPC demonstrates the capability of high-quality phase reconstruction because it retrieves a pupil function that is consistent with the ground truth. Thus, the resulting PTF accurately characterizes the quantitative transfer relationship between the intensity signal and the phase of the object. In order to demonstrate the adaptability of ACDPC to different aberrations, we randomly generated ten aberrations and performed ten ACDPC iterations for each of them to statistically analyze the average iteration times and the RMSE of the reconstructed phases. The initial aberration is randomly generated and a random perturbation term with exponential decay properties is dynamically superimposed at each iterative update. As explained in Fig. 3(c), ACDPC at different aberrations converges to a stable value for about 2000 iterations. In addition, the RMSE of the reconstructed phase wit the ground truth is concentrated around a small value, which means that the iterative process will always converge to a result that is consistent with the ground-truth phase. This statistical consistency confirms the stable convergence characteristics of ACDPC in phase retrieval applications.

In order to assess the performance of ACDPC under more complex aberrations, we further simulated multi-order aberrations for comparison. ACDPC well corrects the reconstruction phase artifacts and restores the detail information (Fig. 3(d)). As can be seen in Fig. 3(f), the reconstruction under the conventional DPC deviates significantly from the true phase value, while ACDPC ideally attains a lateral resolution of up to 345 nm (theoretical resolution). Figure 3(g) gives the retrieved aberration coefficients and the given truth coefficients, and the results show that they are in good agreement. The simulation results indicate that ACDPC is capable of accurately recovering multi-order aberrations to cope with the task of high-quality QPI under complex optical systems.

Results

Experiment on USAF resolution target

To demonstrate the performance of the proposed method on a real imaging system, ACDPC was implemented in a commercial inverted microscope (Olympus inverted microscope IX73) by replacing the light source with a programmable LED array. It was controlled via an FPGA to produce three annular illumination patterns with an illumination wavelength of 505 nm. The light field passing through the object is collected by an objective lens with 10×, 0.25 NA and finally imaged on an industrial camera with pixel size of 1.67 μm (The imaging

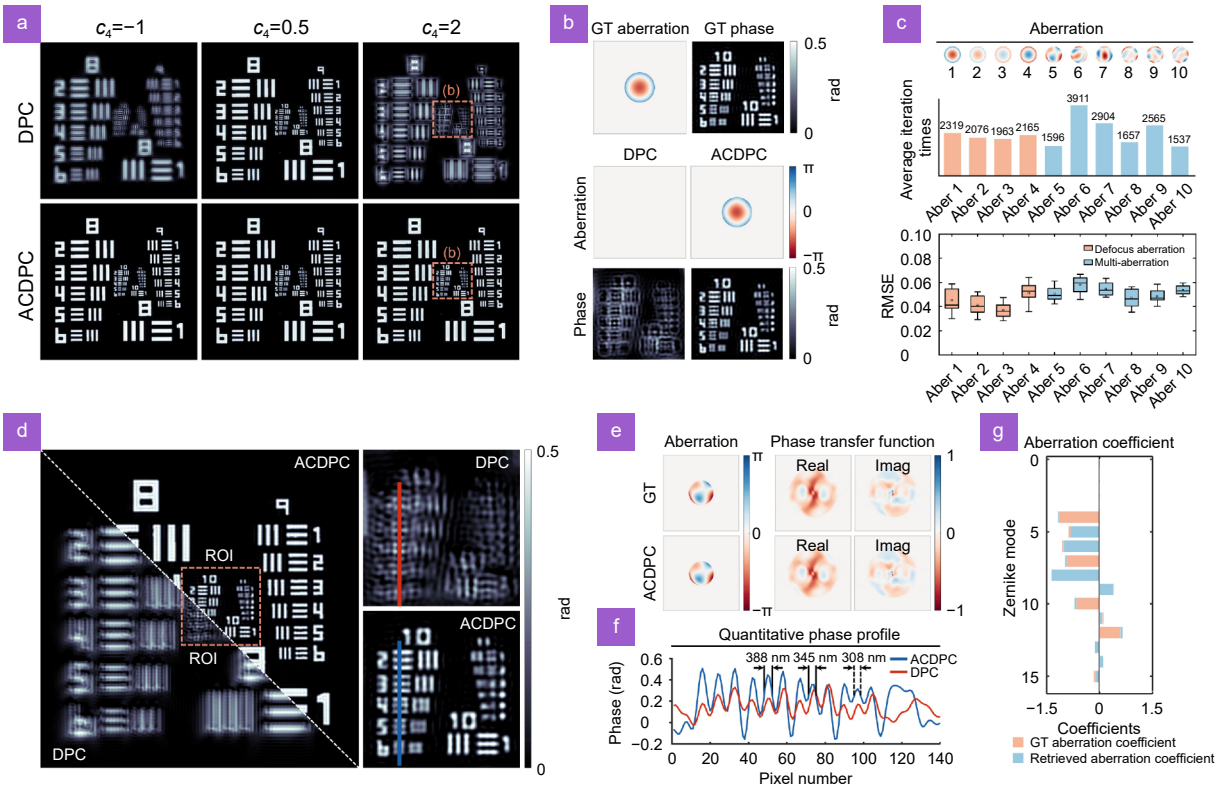

Fig. 3 | Simulation of DPC and ACDPC reconstructed phases with different aberrations. (**a**) Reconstructed phases of DPC and ACDPC with different degrees of defocus aberration. (**b**) Original and retrieved pupils and corresponding reconstructed phase details in defocus aberration. (**c**) Average number of convergence and phase RMSE data for ten aberrations. (**d**) Reconstructed phases of DPC and ACDPC with multi-order aberration. (**e**) Ground-truth pupil and corresponding PTF and ACDPC retrieved pupil and PTF. (**f**) Quantitative profile comparison of reconstructed phase. (**g**) Zernike coefficients for ground-truth and retrieved aberrations.

source DMK 24UJ003). In such a configuration, the expected lateral resolution is 505 nm (half-width resolution), corresponding to Element 6 in Group 9 of the USAF target. By manually adjusting the samples to be located on different defocus planes (−10 μm, +10 μm, +20 μm), we obtained three sets of image data whose aberration levels exceeded those of the actual system. These data were used for the conventional DPC deconvolution reconstruction and ACDPC method, and the results are displayed in Fig. 4. In the original image away from the focal plane, we can observe a loss of detail information, which leads to severe phase blurring and artifacts with DPC reconstruction. This is because the intensity variations due to pupil aberration are incorrectly assigned to the reconstructed phase during the solving process. ACDPC is robust to aberrations at different defocus distances from −10 μm to 10 μm and obtains high-quality reconstructed phases consistent with the focal plane at a large defocus distance. As shown in Fig. 4, ACDPC achieves a lateral resolution of 505 nm, and imaging artifacts and distortions are effectively eliminated. Although there is a degradation in the reconstruction quality of ACDPC at larger aberrations (+20 μm), it is effective in improving the reconstructed resolution and quality compared to the conventional DPC method (Fig. 4(e)).

Experiment on biological cells

DPC technique achieves theoretical resolution of the incoherent diffraction limit, facilitating high-resolution visualization and observation of subcellular structures within cells. Nevertheless, the aberrations may introduce imaging distortions, impeding the full realization of theoretical resolution and obscuring the fine structural details within the cell. To demonstrate the effectiveness of ACDPC for biological cells, we conducted an experiment on NIH 3T3 cells (Mouse Embryonic Fibroblasts). 3T3 cells were cultured using DMEM medium (Gibco, CA, USA). DMEM mediun were added with 10% fetal bovine serum (fBS) and 1% penicilin/streptomycin. All cells were cultured at a temperature of 37 °C in ahumidified atmosphere with 5% CO_2[48]. Cells were fixed with 4% paraformaldehyde (Solarbio, Beijing, China) after 48 h

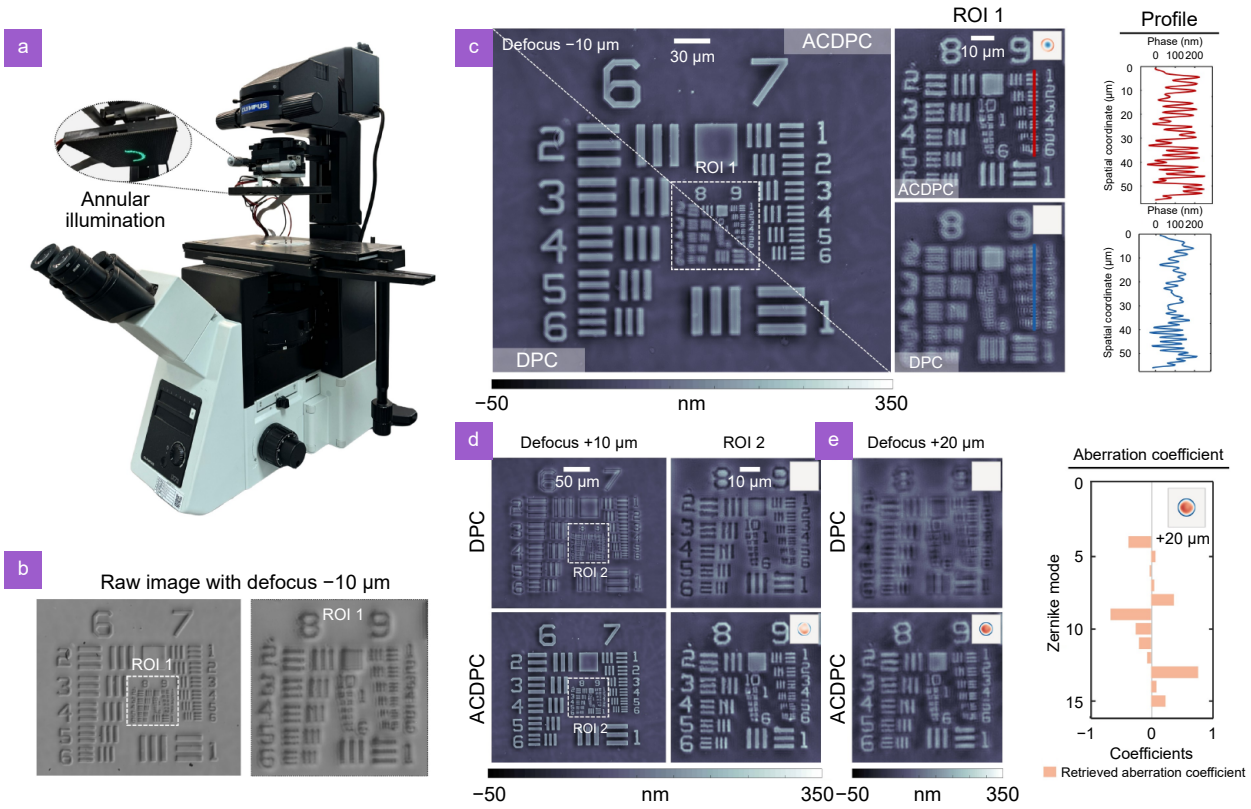

Fig. 4 | Experimental results of USAF resolution targets. (**a**) ACDPC experimental system based on commercial inverted microscope with annular illumination. (**b**) The actual acquired intensity image and the zoom-in image of region of interest (ROI 1). (**c**) Full-field-of-view reconstructed phase and zoom-in images (ROI 1) of DPC and ACDPC at −10 μm defocus, and quantitative phase profile. (**d**) Reconstructed phase and zoom-in images (ROI 2) of DPC and ACDPC at +10 μm defocus. (**e**) Reconstructed phase of DPC and ACDPC at +20 μm defocus and the retrieved aberration coefficient.

culture. In the acquisition process, the cells were placed in the same experimental system as described above, and two sets of intensity images were recorded by manually adjusting the focus to introduce different defocus aberrations for both regions. They are used to perform the DPC and ACDPC methods, and their results are shown in Fig. 5. We utilized the graphics processing unit (GPU) to highly parallelize the execution of ACDPC, which allows us to extract morphological parameters at the cellular level across the entire field of view with 4 min. It can be found that despite manual adjustments to focus the cell sample as much as possible, the actual imaging results of DPC still suffer from aberration damage. Observing the subcellular structure of the cells in the two regions of interest (ROI) in Fig. 5(a), it can be clearly seen that the aberration under DPC leads to the confusion of cellular lipid droplet and cytodesma. ACDPC efficiently retrieved the systematic aberration and obtained a clearly defined, artifact-free cell structure. The results of Fig. 5(b) demonstrate a more severe loss of detail, and its ROI can clearly demonstrate the comparison of the reconstruction results of DPC and ACDPC on the subcellular structure of the cell. Notice that the aberrations retrieved from the two sets of experimental results have a similar distribution due to the use of the same experimental system, while the larger Zernike coefficients in Fig. 5(d) imply more severe defocusing. This can likewise be found by comparing the clarity of the phase of Fig. 5(a) and 5(d). To further validate the time-varying aberration correction capability of ACDPC, we conducted a dynamic experiment on in vitro cultured HeLa cells (The result can be seen in the Supplementary Movie S2). The results demonstrate that ACDPC effectively mitigates time-varying aberrations while enabling high-fidelity quantitative phase reconstruction.

Conclusions

We have proposed an artifact-free aberration-corrected DPC (ACDPC) algorithm empowering QPI microscopy with high robustness against aberration. When

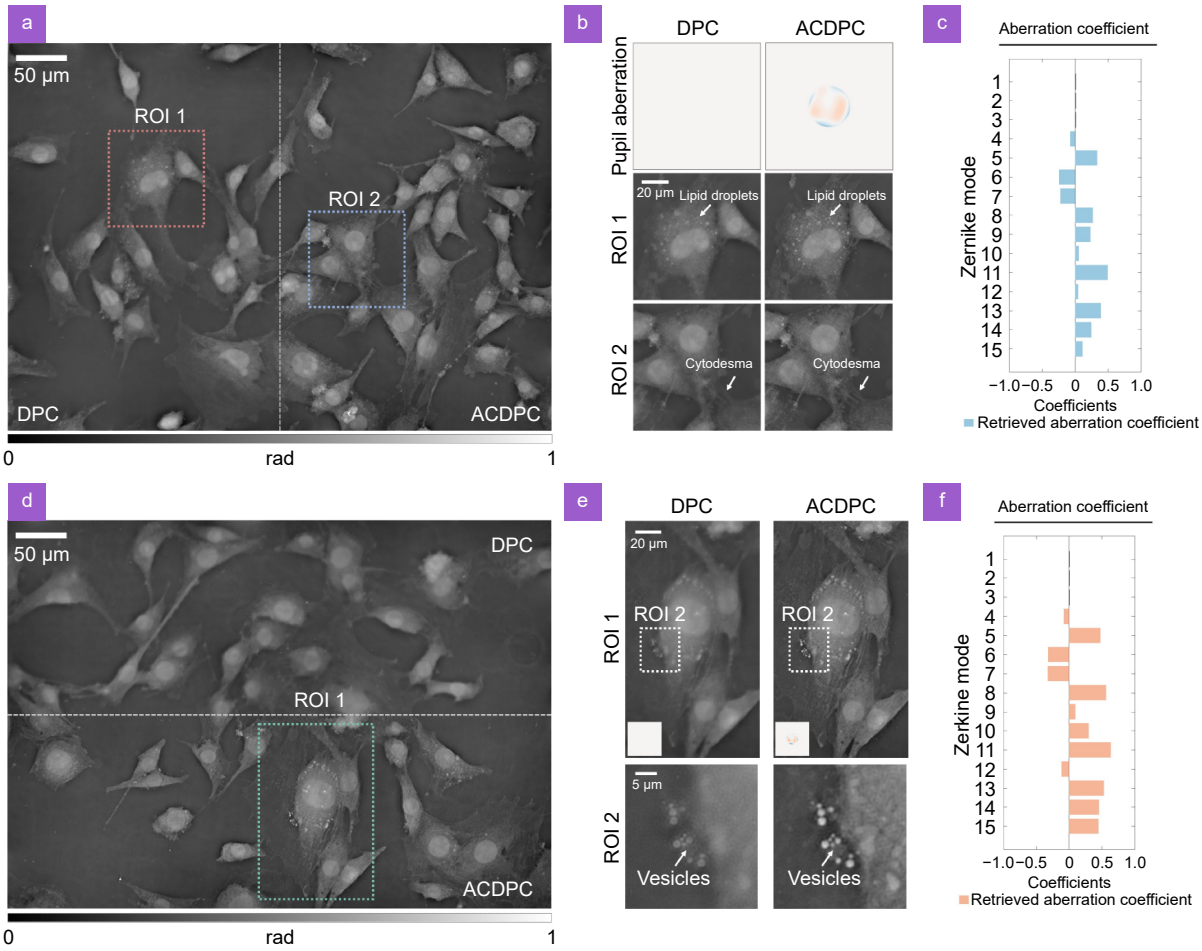

Fig. 5 | Experimental results of DPC and ACDPC on NIH 3T3 cells. (**a**) Experimental result of DPC and ACDPC experiments on NIH 3T3 cell samples under fine focusing conditions. (**b**) Magnified images of two ROIs (ROI 1, ROI 2) in (a). (**c**) Zernike coefficient of retrieved aberration in (b). (**d**) Experimental result of DPC and ACDPC experiments on NIH 3T3 cell samples under coarse focusing conditions. (**e**) Magnified image of the ROI (ROI 1) in (a) and further magnification of its ROI (ROI 2). (**f**) Zernike coefficient of retrieved aberration in (e).

aberrations are present, conventional DPC incorrectly assign aberrations to reconstructed phases, resulting in phase artifacts and blurring. ACDPC employs annular illumination to optimize the PTF, providing a numerically enhanced phase transfer response to ensure that the signal is recorded with a greater SNR. The simulated annealing algorithm and the deconvolution reconstruction are combined to achieve both aberration retrieval and phase restoration without any priori knowledge. In addition, minimal data redundancy to achieve high quality phase reconstruction and aberration correction was also analyzed. Therefore, instead of acquiring additional images under coherent illumination to record aberration information, as in the existing aberration correction DPC method, ACDPC can achieve high-quality phase reconstruction and aberration correction by utilizing only three images under annular illumination. Experiments with USAF resolution targets and NIH 3T3 cells demonstrated the superior aberration correction capability of ACDPC to reproduce the quantitative phase distribution of the sample without artifacts under realistic experimental conditions. These advantages make ACDPC promising for biological cell imaging applications.

It should be emphasized that this manuscript focuses on aberration-corrected DPC QPI, whose validity domain is confined to samples satisfying the weak object approximation (WOA) for quantitative characterization of morphological features. In contrast, for thick specimens violating this approximation, the reconstruction framework must be extended by incorporating scattering-informed imaging models into 3D diffraction tomography (3D-DT). We are continuing to explore the potential of aberration-correction strategies in this advanced modality to achieve high-fidelity refractive index

distribution reconstruction across complex volumetric specimens. Notably, while the proposed method achieves imaging resolution at the incoherent diffraction limit, it exhibits inherent compatibility with advanced super-resolution strategies such as synthetic aperture imaging and microsphere-assisted near-field enhancement[49–51]. This synergistic integration provides a promising pathway to transcend existing resolution boundaries in label-free microscopy, which constitutes a primary objective for our future research endeavors.

References

1. Zernike F. Phase contrast. *Z Tech Physik* **16**, 454 (1935).
2. Evanko D, Heinrichs A, Rosenthal C. Milestones in light microscopy. *Nat Cell Biol* **11**, 1165 (2009).
3. Stephens DJ, Allan VJ. Light microscopy techniques for live cell imaging. *Science* **300**, 82–86 (2003).
4. Qian JM, Cao Y, Bi Y et al. Structured illumination microscopy based on principal component analysis. *eLight* **3**, 4 (2023).
5. Evanko D. Label-free microscopy. *Nat Methods* **7**, 36 (2010).
6. Fan Y, Li JJ, Lu LP et al. Smart computational light microscopes (SCLMs) of smart computational imaging laboratory (SCILab). *PhotoniX* **2**, 19 (2021).
7. Küppers M, Albrecht D, Kashkanova AD et al. Confocal interferometric scattering microscopy reveals 3D nanoscopic structure and dynamics in live cells. *Nat Commun* **14**, 1962 (2023).
8. Kemper B, Bauwens A, Vollmer A et al. Label-free quantitative cell division monitoring of endothelial cells by digital holographic microscopy. *J Biomed Opt* **15**, 036009 (2010).
9. Liu SQ, Yu FH, Hong R et al. Advances in phase-sensitive optical time-domain reflectometry. *Opto-Electron Adv* **5**, 200078 (2022).
10. Fienup JR. Phase retrieval algorithms: a comparison. *Appl Opt* **21**, 2758–2769 (1982).
11. Popescu G. *Quantitative Phase Imaging of Cells and Tissues* (McGraw-Hill, New York, 2011).
12. Park Y, Depeursinge C, Popescu G. Quantitative phase imaging in biomedicine. *Nat Photon* **12**, 578–589 (2018).
13. Kim T, Zhou RJ, Goddard LL et al. Solving inverse scattering problems in biological samples by quantitative phase imaging. *Laser Photon Rev* **10**, 13–39 (2016).
14. Huang ZZ, Memmolo P, Ferraro P et al. Dual-plane coupled phase retrieval for non-prior holographic imaging. *PhotoniX* **3**, 3 (2022).
15. Gao P, Yao BL, Harder I et al. Phase-shifting Zernike phase contrast microscopy for quantitative phase measurement. *Opt Lett* **36**, 4305–4307 (2011).
16. Hamilton DK, Sheppard CJP. Differential phase contrast in scanning optical microscopy. *J Microsc* **133**, 27–39 (1984).
17. Mehta SB, Sheppard CJR. Quantitative phase-gradient imaging at high resolution with asymmetric illumination-based differential phase contrast. *Opt Lett* **34**, 1924–1926 (2009).
18. Bertero M, Boccacci P, De Mol C. *Introduction to Inverse Problems in Imaging* (CRC Press, Boca Raton, 2021).
19. Tian L, Waller L. Quantitative differential phase contrast imaging in an led array microscope. *Opt Express* **23**, 11394–11403 (2015).
20. Chen HH, Lin YZ, Luo Y. Isotropic differential phase contrast microscopy for quantitative phase bio-imaging. *J Biophoton* **11**, e201700364 (2018).
21. Fan Y, Sun JS, Shu YF et al. Accurate quantitative phase imaging by differential phase contrast with partially coherent illumination: beyond weak object approximation. *Photon Res* **11**, 442–455 (2023).
22. Hamilton DK, Sheppard CJR, Wilson T. Improved imaging of phase gradients in scanning optical microscopy. *J Microsc* **135**, 275–286 (1984).
23. Gao P, Yao BL, Min JW et al. Autofocusing of digital holographic microscopy based on off-axis illuminations. *Opt Lett* **37**, 3630–3632 (2012).
24. Song PM, Jiang SW, Zhang H et al. Full-field Fourier ptychography (FFP): spatially varying pupil modeling and its application for rapid field-dependent aberration metrology. *APL Photon* **4**, 050802 (2019).
25. Kam Z, Hanser B, Gustafsson MG et al. Computational adaptive optics for live three-dimensional biological imaging. *Proc Natl Acad Sci USA* **98**, 3790–3795 (2001).
26. South FA, Liu YZ, Bower AJ et al. Wavefront measurement using computational adaptive optics. *J Opt Soc Am A* **35**, 466–473 (2018).
27. Zheng GA, Ou XZ, Horstmeyer R et al. Characterization of spatially varying aberrations for wide field-of-view microscopy. *Opt Express* **21**, 15131–15143 (2013).
28. Horstmeyer R, Ou XZ, Chung J et al. Overlapped Fourier coding for optical aberration removal. *Opt Express* **22**, 24062–24080 (2014).
29. Bostan E, Heckel R, Chen M et al. Deep phase decoder: self-calibrating phase microscopy with an untrained deep neural network. *Optica* **7**, 559–562 (2020).
30. Goda K, Popescu G, Tsia KK et al. Computational optical imaging goes viral. *APL Photon* **5**, 030401 (2020).
31. Li ZS, Chen YY, Sun JS et al. High bandwidth-utilization digital holographic reconstruction using an untrained neural network. *Appl Sci* **12**, 10656 (2022).
32. Zheng GA, Horstmeyer R, Yang CH. Wide-field, high-resolution Fourier ptychographic microscopy. *Nat Photon* **7**, 739–745 (2013).
33. Ou XZ, Zheng GA, Yang CH. Embedded pupil function recovery for Fourier ptychographic microscopy. *Opt Express* **22**, 4960–4972 (2014).
34. Shu YF, Sun JS, Lyu JM et al. Adaptive optical quantitative phase imaging based on annular illumination Fourier ptychographic microscopy. *PhotoniX* **3**, 24 (2022).
35. Lu LP, Li JJ, Shu YF et al. Hybrid brightfield and darkfield transport of intensity approach for high-throughput quantitative phase microscopy. *Adv Photon* **4**, 056002 (2022).
36. Chen M, Phillips ZF, Waller L. Quantitative differential phase contrast (DPC) microscopy with computational aberration correction. *Opt Express* **26**, 32888–32899 (2018).
37. Sun JS, Zuo C, Zhang JJ et al. High-speed Fourier ptychographic microscopy based on programmable annular illuminations. *Sci Rep* **8**, 7669 (2018).
38. Fan Y, Sun JS, Chen Q et al. Optimal illumination scheme for isotropic quantitative differential phase contrast microscopy. *Photon Res* **7**, 890–904 (2019).
39. Cao RZ, Shen C, Yang CH. High-resolution, large field-of-view label-free imaging via aberration-corrected, closed-form com-

plex field reconstruction. *Nat Commun* **15**, 4713 (2024).
40. Fan Y, Sun JS, Chen Q et al. Single-shot isotropic quantitative phase microscopy based on color-multiplexed differential phase contrast. *APL Photon* **4**, 121301 (2019).
41. Sasian J. *Introduction to Aberrations in Optical Imaging Systems* (Cambridge University Press, Cambridge, 2012).
42. Booth MJ. Adaptive optics in microscopy. *Philos Trans A Math Phys Eng Sci* **365**, 2829–2843 (2007).
43. Zernike F, Nijboer B. Theorie de la diffraction des aberrations. *La Theorie des Images Optiques* 227–235 (1949).
44. Wyant JC, Creath K. Basic wavefront aberration theory for optical metrology. *Appl Opt Opt Eng* **11**, 28–39 (1992).
45. Lakshminarayanan V, Fleck A. Zernike polynomials: a guide. *J Mod Opt* **58**, 545–561 (2011).
46. Zhou S, Li JJ, Sun JS et al. Transport-of-intensity Fourier ptychographic diffraction tomography: defying the matched illumination condition. *Optica* **9**, 1362–1373 (2022).
47. Lenzen F, Scherzer O. Tikhonov type regularization methods: history and recent progress. In *Proceedings of European Congress on Computational Methods in Applied Sciences and Engineering* 1–21 (ECCOMAS, 2004).
48. Sargis RM, Johnson DN, Choudhury RA et al. Environmental endocrine disruptors promote adipogenesis in the 3T3-L1 cell line through glucocorticoid receptor activation. *Obesity* **18**, 1283–1288 (2010).
49. Chen LW, Zhou Y, Li Y et al. Microsphere enhanced optical imaging and patterning: from physics to applications. *Appl Phys Rev* **6**, 021304 (2019).
50. Boneberg J, Leiderer P. Optical near-field imaging and nanostructuring by means of laser ablation. *Opto-Electron Sci* **1**, 210003 (2022).
51. Chu CY, Liu ZT, Chen ML et al. Wide-spectrum optical synthetic aperture imaging via spatial intensity interferometry. *Opto-Electron Adv* **6**, 230017 (2023).

Acknowledgements

This work was supported by the National Natural Science Foundation of China (62305162, 62227818, 62361136588), China Postdoctoral Science Foundation (2023TQ0160, 2023M731683), Nanjing University of Science and Technology independent research project (30923010305), National Key Research and Development Program of China (2024YFE0101300), Biomedical Competition Foundation of Jiangsu Province (BE2022847), Key National Industrial Technology Cooperation Foundation of Jiangsu Province (BZ2022039), Fundamental Research Funds for the Central Universities (2023102001), and Open Research Fund of Jiangsu Key Laboratory of Spectral Imaging & Intelligent Sense (JSGP202105, JSGP202201, JSGPCXZNGZ202401). The authors thank Feng Wei from Smart Computational Imaging Research Institute (SCIRI) of Nanjing University of Science and Technology for preparing the NIH 3T3 cell samples.

Author contributions

Yao Fan proposed the initial concept and drafted the initial manuscript. Chenyue Zheng implemented and conducted experimental validation. Yefeng Shu and Qingyang Fu participated in discussions regarding the algorithms and revisions of the manuscript. Lixiang Xiong and Guifeng Lu were involved in the experiments and the creation of figures for the manuscript. Jiasong Sun, Chao Zuo, and Qian Chen jointly oversaw the progress of the entire project and provided guiding insights.

Competing interests

The authors declare no competing financial interests.

Supplementary information

Supplementary information for this paper is available at https://doi.org/10.29026/oes.2025.240037